Article DOI: https://doi.org/10.37284/ijar.5.1.677

International Journal of Advanced Research
ijar.eanso.org
Volume 5, Issue 1, 2022
Print ISSN: 2707-7802 | Online ISSN: 2707-7810
Title DOI: https://doi.org/10.37284/2707-7810

EAST AFRICAN NATURE & SCIENCE ORGANIZATION

Original Article

Synthesis of Topped $ZnSeO_4$ QDs and their Evaluation as Chemical Nanosensors for Anthracene, Benzo (A) Pyrene, Pyrene and Pyridine

Pamela Khakasa Butalanyi[1], Jackson Kiptoo[1], Anam Onditi[1], Dickson Andala[2], Wallace Bulimo[3], Benson K. Mwanza[3] & John K. Muchuna[1]*

[1] Jomo Kenyatta University of Agriculture and Technology, P. O. Box 62000-00100, Nairobi, Kenya.
[2] Multimedia University, P. O. Box 15653-00503, Nairobi, Kenya.
[3] University of Nairobi, P. O. Box 30197-00100, Nairobi, Kenya.
* Author for Correspondence ORCID ID: https://orcid.org/0000-0003-0626-4421; Email: butalanyipk@googlemail.com.

Article DOI: https://doi.org/10.37284/ijar.5.1.677

Publication Date:

21 May 2022

Keywords:

Fluorescence Based Fibre Optical Chemical Nano-Sensor, Carcinogenic Organic Pollutants, Znseo4-Hexamine Capped Qds, Vehicle Exhaust Dust Extract, Cigarette Smoke Extract.

ABSTRACT

Synthesis and characterization of hexamine capped $ZnSeO_4$ QDs ($ZnSeO_4$-Hex) by heating up method (HU) was achieved. These, of two crystallite sizes, denoted QDsS1 and QDsS2; with crystallite diameters of 8.6 nm and 14.0 nm respectively. X-ray diffraction (XRD) pattern bared hexagonal close packed (hcp) crystal structure. Band gap for QDsS1 was 5.85 eV and for QDsS2 3.8 to 4.3 eV. Hexamine ($C_6H_{10}N_4$) cap on $ZnSeO_4$ QDs was elucidated by Fourier Transform Infrared Spectroscopy (FTIR) and Gas Chromatography-Mass Spectroscopy (GC-MS) results. Transmission Electron Microscopy (TEM) images revealed polycrystallites of different orientation, showing crystal grains separated by tilted grain boundary folds. These QDs were tested as optical chemical nano-sensors for carcinogenic organic pollutants: Anthracene (ANTH), Benzo (a) pyrene (BaP), pyrene (PRN) and pyridine (py). Results revealed that, when the organic pollutants interacted with the QDs, they caused characteristic changes in the way these nanoparticles interacted with characteristic fluorescence and absorbance spectrum.

APA CITATION

Butalanyi, P. K., Kiptoo, J., Onditi, A., Andala, D., Bulimo, W., Mwanza, B. W., & Muchuna, J. K. (2022). Synthesis of Topped ZnSeO4 QDs and their Evaluation as Chemical Nanosensors for Anthracene, Benzo (A) Pyrene, Pyrene and Pyridine. *International Journal of Advanced Research*, *5*(1), 60-83. https://doi.org/10.37284/ijar.5.1.677

CHICAGO CITATION

Butalanyi, Pamela Khakasa, Jackson Kiptoo, Anam Onditi, Dickson Andala, Wallace Bulimo, Benson K. Mwanza and John K. Muchuna. 2022. "Synthesis of Topped ZnSeO4 QDs and their Evaluation as Chemical Nanosensors for Anthracene, Benzo (A) Pyrene, Pyrene and Pyridine." *International Journal of Advanced Research* 5 (1), 60-83. https://doi.org/10.37284/ijar.5.1.677.

Article DOI: https://doi.org/10.37284/ijar.5.1.677

HARVARD CITATION

Butalanyi, P. K., Kiptoo, J., Onditi, A., Andala, D., Bulimo, W., Mwanza, B. W., & Muchuna, J. K. (2022) "Synthesis of Topped ZnSeO4 QDs and their Evaluation as Chemical Nanosensors for Anthracene, Benzo (A) Pyrene, Pyrene and Pyridine.", *International Journal of Advanced Research*, 5(1), pp. 60-83. doi: 10.37284/ijar.5.1.677.

IEEE CITATION

P. K. Butalanyi., J. Kiptoo., A. Onditi., D. Andala., W. Bulimo., B. K. Mwanza., & J. K. Muchuna, "Synthesis of Topped ZnSeO4 QDs and their Evaluation as Chemical Nanosensors for Anthracene, Benzo (A) Pyrene, Pyrene and Pyridine.", *IJAR*, vol. 5, no. 1, pp. 60-83, May. 2022.

MLA CITATION

Butalanyi, Pamela Khakasa, Jackson Kiptoo, Anam Onditi, Dickson Andala, Wallace Bulimo, Benson K. Mwanza & John K. Muchuna. "Synthesis of Topped ZnSeO4 QDs and their Evaluation as Chemical Nanosensors for Anthracene, Benzo (A) Pyrene, Pyrene and Pyridine.". *International Journal of Advanced Research*, Vol. 5, no. 1, May. 2022, pp. 60-83, doi:10.37284/ijar.5.1.677.

INTRODUCTION

Compounds namely; anthracene (ANTH), benzo(a)pyrene (BaP), pyrene (PRN) and pyridine (py) are carcinogenic. Apart from pyridine, all the above compounds are Polycyclic Aromatic Hydrocarbons (PAHs) and they occur naturally in coal, crude oil and gasoline and they are also produced by the incomplete combustion of coal, oil, gas, garbage, and tobacco. Many products including roofing tar, certain dyes, and pesticides, contain PAHs. These harmful chemicals therefore, find their way into the atmosphere from vehicle exhaust emissions, from residential and industrial furnaces, tobacco smoke, volcanoes, and forest fires. During emission, these pollutants may attach onto surfaces in the environment and in the air, and by so doing, contaminate surface and groundwater accessible by living organisms. Pyridine is also found in mixtures of these PAHs. According to the International Agency for Research on Cancer (IARC), the National Toxicology Program (NTP), and the U.S. Environmental Protection Agency (EPA), these pollutants have been classified as definite carcinogens. Some people who have breathed or touched mixtures of PAHs for long periods have developed cancer. In laboratory animals, some PAHs have caused lung, stomach, or skin cancer (Rengarajan et al., 2015). PAHs are lipophilic and therefore they easily form adducts with DNA in animal tissues (Chard et al., 2001, Koganti et al., 2001, Pierre et al., 1996). They are therefore harmful compounds to humans and animals, hence, least desired in the environment.

Since these organic chemicals are toxic, Environmental Protection Agency (EPA), World Health Organization (WHO), Occupational Safety and Health Administration (OSHA), Agency for Toxic Substances and Disease Registry (ATSDR) and National Institute for Occupational Safety and Health (NIOSH) among many environmental monitoring agencies in the world have set Permissible Exposure limits (PEL), dissolved in drinking water and airborne, which they deem through research, to be less harmful (NIOSH Manual 1986). Presented in *Table 1* are PEL from some of the environmental monitoring agencies.

Table 1: PEL for ANTH, BaP, PRN and Py

AGENCY	PEL		Parts per billion (ppb)
	Air (mg/m^3)	Water (mg/L)	
ATSDR	0.2	*0.0002*	*0.2*
EPA	0.2	*0.0002*	*0.2*
NIOSH	0.1	*0.0001*	*0.1*
OSHA	0.2	*0.0002*	*0.2*

*PEL for pyridine 5 ppm and 15 mg/m^3. *Asterisks show same concentration converted from mg/L to ppb.*

Article DOI: https://doi.org/10.37284/ijar.5.1.677

The data in *Table 1* was sourced from the listed agencies' websites.

BACKGROUND

Chemical Sensors

Considerable research has previously been carried out on optical fibre based gas and vapour sensing, which utilized chemical sensors such as: porphyrin films (Yusoff et al., 2008), metallophthalocyanines (Granito et al., 1996; Lloyd et al., 1987; Spadaveccha et al., 2004) inorganic metal oxides (Körber et al., 2002; Niranjan et al., 2002), semiconductors (Horrillo et al., 1998), carbon nanotubes (Li et al., 2003; Penza et al., 2005; Quercia et al., 2004), calixarenes (Kalchenko et al., 2002; Koshets et al., 2005), zeolites (Dubbe et al., 2006; Mintova et al., 2001; Vilaseca et al., 2003; Zhang et al., 2006), polymers (Fort et al., 2005; Shepherd et al., 2002; Sluszny et al., 2004) and molecularly imprinted polymers (Chen et al., 2004; Dickert et al., 1998; Wolfbeis et al., 1988).

Semi-conductor nanoparticles (NPs) application in various scientific fields including sensing, has been an area of great interest for research scientists. Various methods have been employed in synthesis and assembly of these nanoparticles. Some of the methods employed in synthesis include: Solvothermal synthesis method *(*Srivastava et al., 2012*)*; chemical precipitation method *(*Amiri et al., 2013*)*; microwave method *(*Amiri et al., 2011*)*; hot injection method *(*Pradhan et al., 2007; Steckel et al., 2006*)*; sonochemical method *(*Zhu et al., 2000*)* and heating up method *(*Yang et al., 2005; Yu et al., 2005*)*. Previously, NPs have been synthesized in aqueous media *(*Zhu et al., 2000*)*. In recent years, preparation in organic solvents has been achieved *(*Wang et al., 2010; Reis et al., 2004; Hines et al., 1998*)*.

In this study the authors applied heating up method to synthesize $ZnSeO_4$, which was capped with hexamine; abbreviated as: ($ZnSeO_4$-hex), and these chemicals were also exploited in this research as optical nano-chemical sensors.

EXPERIMENTAL

Quantum Dots Synthesis

Synthesis of QDsS1 and QDsS2 was carried out by Heating-Up method in 100 ml deionized water solution containing 2.94 g $ZnSO_4.7H_2O$, 2.80 g SeO_2 and 1.5 g hexamine ($C_6H_{12}N_4$). As reported in literature, a clean three necked 250 ml refluxing synthesis flask was loaded with the above chemicals and deionized water and all accessories assembled. The contents were placed on heated sand bath; over a hot plate and the temperature adjusted to 300 ^{0}C which is appropriate for synthesis of these QDs. After the contents inside the flask started boiling, refluxing was continued for 1 hr. and 45 min. at lower temperature of 250 ^{0}C. The temperature was lowered so as to avoid any decomposition of the products and also convenient for crystal growth. Fine white fluffy crystals formed, turned minute, pale pink crystallites with continued refluxing and a clear colourless solution above the crystallites. The crystals were isolated and labelled QDsS1. The supernatant was then evaporated and crystals of similar colour as above recovered and labelled as QDsS2 - these had a tendency to further crystallize forming needle like crystals of the same pale pink colour. This synthesis therefore gave the authors two crystal types.

Quantum Dots Characterization

Instrumental spectroscopic methods for characterization of QDs included: Absorption spectroscopy (AS), Gas Chromatography – Mass Spectroscopy (GC-MS), Fourier Transform Infra-Red spectroscopy (FTIR), Total X-ray fluorescence spectroscopy (TXFS), Energy Dispersive X-ray (EDX), X-ray Diffraction spectroscopy (XRD and Transmission Electron Microscopy (TEM).

Absorption

The QDs $ZnSeO_4$-Hex (QDsS1 and QDsS2), were soluble in nitric acid or water/nitric acid solvent combination of three parts water and 1-part nitric acid (3:1). Initially, 1.8 g of the nanoparticles, QDsS1, were dissolved in 100:3 ml deionized water to nitric acid respectively. Similarly, QDsS2 were prepared and the absorption spectra for the two crystallite sizes of $ZnSeO_4$-Hex were recorded.

Article DOI: https://doi.org/10.37284/ijar.5.1.677

Absorbance data was used in estimation of molecular weight (MW) for $ZnSeO_4$-Hex. The standards were prepared by mixing 0.5 mmol of SeO_2, mixed with 0.5 mmol $ZnSO_4.7H_2O$ in 100 ml deionized water and the dilutions from the standards of: 0.05, 0.1, 0.15, 0.2 and 0.25 mmol concentrations were prepared and absorption data measured – the signals for these concentrations are presented in the results section. Estimation of the QDs band gaps was from absorbance data and the spectra for this are presented in results' section.

Energy dispersive X-ray Spectroscopy (EDX) and Total X-ray Fluorescence Spectroscopy (TFXS)

Energy Dispersive X-ray study, the samples were analysed on Shimadzu Rayny EDX 800HS at the ministry of transport - Kenya, materials' department, and the analysis for Total X-ray Fluorescence Spectroscopy (TFXS), was achieved using S2 PICOFOX TXRF spectrometer at the institute of Nuclear Science of the University of Nairobi.

Shimadzu Rayny EDX 800HS

Prior to analysis, liquid nitrogen was placed inside its chamber in the instrument. The work of liquid nitrogen was for cooling the detector (-180 to -186 ^{0}C). The amount of sample, 5 mg was smeared on a Mylar thin film and placed directly over the aperture that allows the X-rays inside the analyte chamber, striking the sample from below. The computer interface to the EDX was set so that the software for the purpose of such analyses could display the data obtained.

S2 PICOFOX TXRF Spectrometer

Solutions for the samples were analysed using TXRFS. The sample of 1 g, was weighed in a clean vial and 10 ml of distilled water was added into the vial, 20 µL of gallium stock solution was added into the vial containing the analyte. Gallium standard was used as internal standard. The concentration of Ga internal standard in the sample was 2 ppm. The sample was then homogenized using a vortex mixer for one minute. Aliquots of 10 µL of the sample were pipetted onto a clean quartz sample holder, using a micropipette. The sample was prepared in triplicate. The triplicate samples were then dried inside the oven and after cooling, they were analysed. Each sample was placed in the sample carrier inside S2 PICOFOX TXRF spectrometer and irradiated for 1000 seconds. This instrument, which uses a molybdenum anode was operated at 50 kV and a current of 1000 µA. The concentrations were calculated based on net intensities of the analyte peak and that of the internal standard using Equation 1.

$$C_a = \frac{N_a/S_a}{N_{is}/S_{is}} \times C_{ix} \quad (1)$$

Where, C_a = Concentration of the analyte, C_{is} = Concentration of the internal standard, N_a Net = intensity of the analyte, N_{is} = Net intensity of the internal standard; S_a =Relative sensitivity of analyte. R =elative sensitivity of internal standard

Gas chromatography

The samples initially dissolved in a few drops of deionized water and nitric acid (3:1); thus, three parts deionized water and one-part nitric acid was diluted using ethanol. The solutions were then analysed using Shimadzu QP GC-MS 2010 -SE, on BPX5 nonpolar column –The samples were placed in glass vials where 1.0 µL of each were dispensed for analysis by GC-MS using auto sampler. The analysis was carried out at Technical University of Kenya.

Fourier transform infra-red spectroscopy (FTIR)

Infra-Red spectroscopy for the QDs was performed on FTIR model WQF 520 with a resolution of 4 and 20 scan times. The sample tablet initially prepared in ratio of 0.01 mg of sample to 0.2 mg of potassium bromide and thoroughly mixed, was ground into fine powder and dried at 70 ^{0}C. During measurement, the sample was held sandwiched between KBr FTIR windows and place inside the sample holder inside the sample chamber of the instrument.

Article DOI: https://doi.org/10.37284/ijar.5.1.677

Transmission electron microscopy

Transmission Electron microscopy (TEM) analysis was carried out on JEM2100F Field Emission TEM (FETEM). Samples for TEM were highly dispersed in ethanol through sonication, then mounted on carbon laced copper grid prior to analysis.

X-ray diffraction spectroscopy

The X-ray diffraction spectra were collected from 10 – 900 2θ, with X-ray wavelength of 1.5406 Å (Copper Kα) radiation source at the rate of 0.50 per minute at room temperature, on a Scintag XDS 2000 θ – θ diffractometer, equipped with a Ge (Li) solid detector. The samples for powder XRD were compacted and were at least 1 mm in thickness to prevent penetration of the X-ray beam.

Identification of a given crystal structure is usually done by correlating the diffraction pattern obtained with known standard diffraction files termed; Joint Committee on Powder Diffraction Standards (JCPDS). X-ray diffraction was an important analytical tool utilized in structure crystallite size and shape determination in the QDs fabricated. The estimation of crystal thickness was achieved using the Scherer Equation 2.

$$t = \frac{0.9\lambda}{BCos\ \theta} \qquad (2)$$

Where; t = the crystal thickness, λ = the wavelength of the X-rays (t and λ have the same units; here in Å), θ = the Bragg's angle, B = the Full-Width at Half-Maximum (FWHM) of the peak in radians, corrected for instrumental broadening

Sensing evaluation for $ZnSeO_4$-Hex (QDsS1 and QDsS2)

Pollutants

Anthracene, benzo (a) pyrene, and pyrene were purchased from Sigma-Aldrich through Kobian Scientific as their agents in Kenya, while pyridine was sourced from R D HAEN through Kobian as their agents and ethanol was obtained from Manigate agencies ltd. These reagents were of analytical grade with high purity and therefore used as purchased, without further purification.

Instruments

Instruments used for evaluation of sensors in this study were Shimadzu 1800 UV-VIS PC spectrophotometer for absorbance and Infinite M 1000 Tecan analyser, for fluorescence measurements.

Absorption and fluorescence study

Known concentrations of solutions for the sensing reagent and those of pollutant molecules were prepared as stocks in appropriate solvents and then dilutions made from them in µM concentrations. Absorption and fluorescence measurements were performed for the solutions of $ZnSeO_4$-Hex alone and fixed concentration of $ZnSeO_4$-Hex with varying concentration of pollutant molecules. Six replicate measurements were carried out on same concentrations for the sensing reagents alone and these sensors with the pollutants so as to establish repeatability of measurements and establish their characteristic peaks before and after interaction – for reference.

Absorbance for $ZnSeO_4$-Hex (QDsS1 and QDsS2) with neat pollutants

The spectra were measured of solutions of neat pollutants alone so as to model calibration curves and subsequently, of neat pollutants after interaction with nano sensors. Aliquots in successive 10 µL were pipetted from the stoke solutions of the pollutants and added in fixed concentration of $ZnSeO_4$-Hex inside quartz cuvette of 1 cm light path length. Each pollutant was measured separately with fixed concentration of the sensing nanoparticles to establish characteristic peaks formed after interaction of a specific pollutant with the nanoparticle sensors.

Fluorescence for $ZnSeO_4$-Hex (QDsS1 and QDsS2) with neat pollutants

Fluorescence measurements and method development were carried out on Tecan M1000 Analyzer. Fixed concentration for the $ZnSeO_4$-Hex as sensing reagent was established visually after a series of measurements for signal to be within the fluorescence scale. The measurements were also performed of the neat pollutants interacting with nano sensors for modelling of calibration plots. The

Article DOI: https://doi.org/10.37284/ijar.5.1.677

solutions were measured using the same procedure as of absorbance, as mentioned earlier, where the nano sensors concentrations were fixed, as the pollutants' concentrations increased in aliquots of 10 µL every successive measurement.

Absorption and fluorescence of vehicle exhaust environmental samples with $ZnSeO_4$-Hex (QDsS1 and QDsS2)

Sampling of cigarette smoke was carried out at a designated smoking zone in Central Business District (CBD) of Nairobi city. The sample was bubbled into a glass vial containing 2 ml of absolute ethanol through a plastic straw. The cigarette smoke was observed inside the stoppered bottle above the ethanol but with vigorous shaking, the smoke went into solution. It formed a colourless solution of cigarette smoke in absolute ethanol. Diesel engine Minibus exhaust pipe dust was scraped from the vehicle's exhaust pipe system, using a spatula, and placed into a clean glass vial. The samples were then preserved well and transported to the laboratory for analysis.

The samples were analysed on a Shimadzu1800 UV-VIS PC spectrophotometer in a quartz cuvette of 1 cm path length and a slit width of 1.5 nm. The constituents of cigarette smoke and diesel engine vehicle exhaust pipe dust dissolved in absolute ethanol. About 5 mg of vehicle exhaust pipe dust was added in ethanol and filtered using a plastic syringe, attached to an acrodisc syringe filter - 0.2 µm HT Tuffryn membrane. The resulting solution of vehicle exhaust pipe dust appeared ochre in colour. Absorption spectra of the solutions for these environmental samples alone were studied, subsequently, the absorption spectra for the samples with the sensor nanoparticles' solutions. Fluorescence studies were accomplished using Infinite M 1000 Tecan Analyser. Samples as prepared for absorbance study were used for fluorescence study. The concentration for QDsS1 ($ZnSeO_4$-Hex of 8.6 nm size) and QDsS2 ($ZnSeO_4$-Hex of 14.0 nm size) was 90.3 µM; 100 µL aliquots of each sensing reagent was placed in individual wells of Corning 96 Flat Bottom Black Polystyrol (COS96fb.pdfx) wells plate. Seven replicate measurements for each, thus of each sensor reagent with cigarette smoke solution and vehicle exhaust pipe extracted solution - 50 µL aliquots of the environmental samples were added to the sensors inside the wells and measurements performed. The excitation wavelength range for QDsS1 was 230 – 300 nm with excitation maximum at 273 nm; wavelength for emission was 398 – 700 nm, with an emission maximum peak at 514 nm and that for QDsS2; excitation was set at 230 nm – 300 nm. The excitation and emission bandwidth(s) were 10 nm and 15 nm respectively. The z-position was manually set at 20000 µm and sample irradiated at 400 Hz flash frequency of 50 flashes with integration time of 20 µs. Initially absorption and fluorescence spectra for the sensors alone had also been acquired for reference.

RESULTS AND DISCUSSION

Results for Characterization of QDs

The absorption spectra for the two crystallites for $ZnSeO_4$-Hex were as presented in *Figure(s) 1* and *2*.

Article DOI: https://doi.org/10.37284/ijar.5.1.677

Figure 1: Absorption spectrum for QDsS1 ($ZnSeO_4$-Hex; crystallite 8.6 nm)

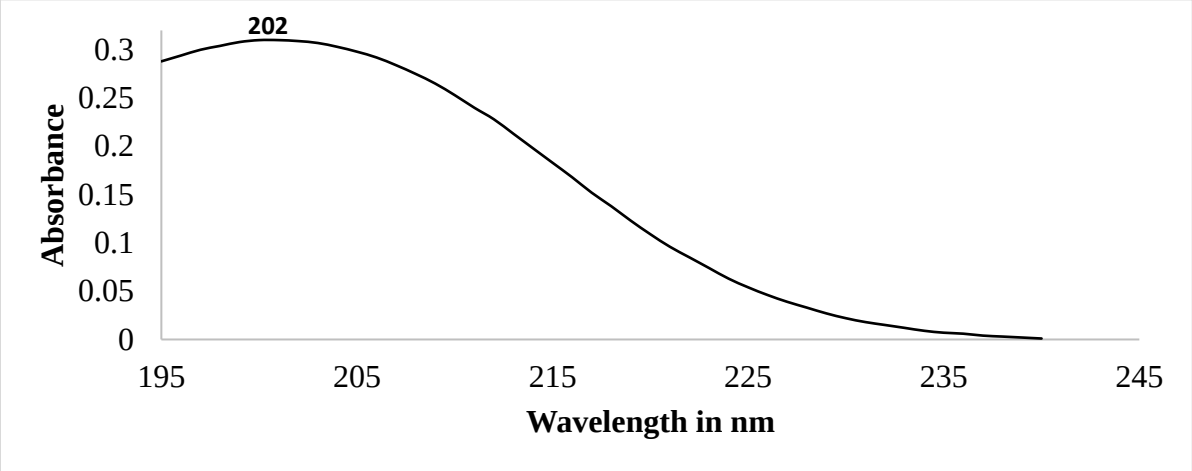

Figure 2: Absorption spectrum for QDsS2 ($ZnSeO_4$-Hex; 14 nm)

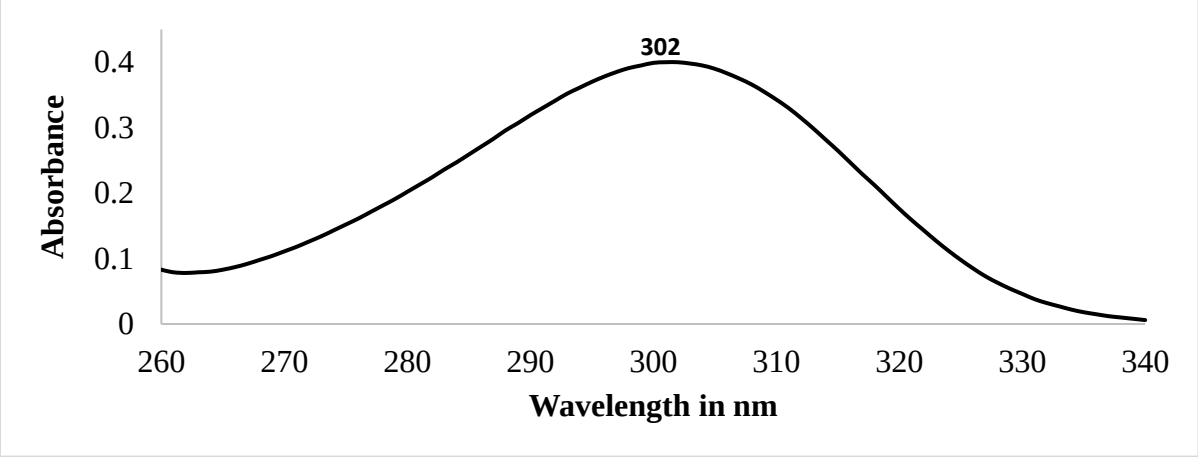

As shown in *Figure 1* and *2*, absorbance for QDsS2 was towards the red end of the electromagnetic spectrum at 302 nm in comparison with that of QDsS1, which was towards the blue end, at 202 nm. As cited in literature, larger QDs crystals absorb at longer wavelengths – thus towards the red end of the electromagnetic spectrum (Goh et al., 2014). This shows that synthesis of two crystals sizes of $ZnSeO_4$–Hex (QDsS1 and QDsS2) was achieved.

Absorption concentrations for estimation of molecular weight for $ZnSeO_4$-Hex were (0.5, 0.1, 0.15, 0.2 and 0.15 whose absorbance signals were (0.196, 0.39, 0.581, 0.75 and 0.875) respectively. The calibration plot(s) were obtained by plotting the signal which is absorbance with corresponding concentration of the standards. As extrapolated from the standards' calibration plot, the molar concentration of QDsS1 was 0.056 mM; initially 1.9 g of $ZnSeO_4$-Hex was used for preparation of the standards and together with molar concentration, they were used to calculate the molecular weight as 339.29 g/mol, but the molecular weight for $ZnSeO_4$-Hex is 348.53 g/mol – this gives an error margin of 2.7 %.

Estimation of band gap for the QDs

Using absorption data, the band gaps for the two crystal sizes QDsS1 and QDsS2 for $ZnSeO_4$-Hex were estimated using the plots as shown in *Figure(s) 3* & *4*.

Article DOI: https://doi.org/10.37284/ijar.5.1.677

Figure 3: Plot of (Ɛhν)^2 vs hν (eV) for estimation of the band gap for QDsS1($ZnSeO_4$-Hex; 8.6 nm size)

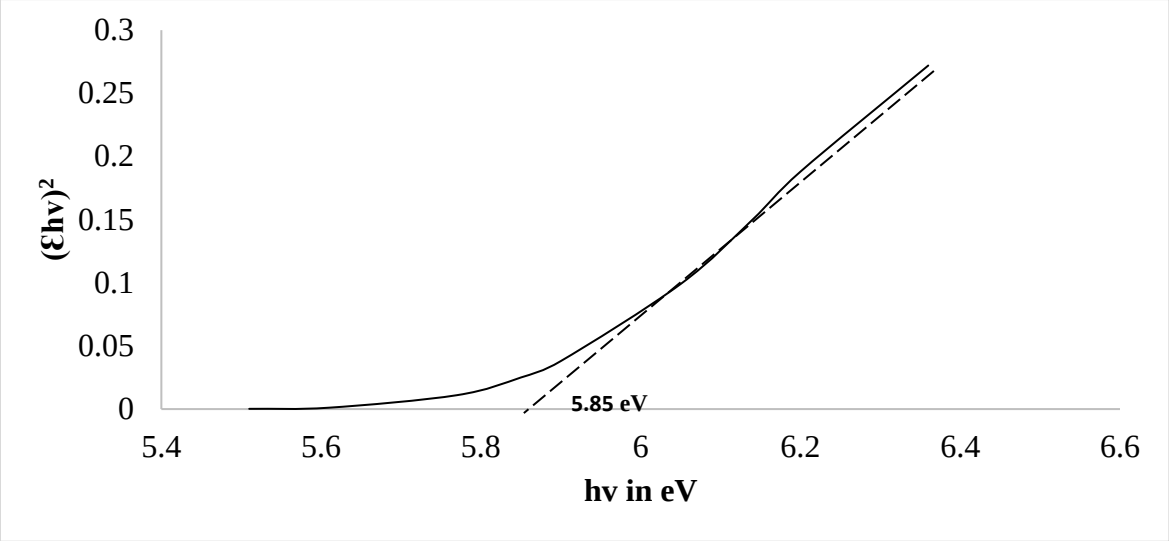

It can be observed that the band gap for QDsS1 is 5.85 eV and that one for QDsS2 is 3.8 - 4.3 eV; ~ 4.01 eV showing that, these nanoparticles were even smaller than uncapped core ZnSe, whose band gap is 2.7 eV as reported in literature (Mosquera et al., 2017). It was established that, QDsS1 and QDsS2 were the same chemically as $ZnSeO_4$ capped with hexamine with different crystallite sizes, where QDsS1 had crystal size of 8.6 nm and QDsS2 had crystal size of 14.0 nm; that is why QDsS1 absorbed at shorter wavelengths of 202 nm, while QDsS2 absorbed at 302 nm. This shift in absorption wavelength conforms to research findings where smaller size nanoparticles absorbed towards the blue end and larger nanoparticles absorbed towards the red end of the electromagnetic spectrum (Goh et al., 2014).

Figure 4: Plot of (Ɛhν)^2 vs hν for estimation of the band gap for QDsS2 ($ZnSeO_4$-Hex; 14 nm size)

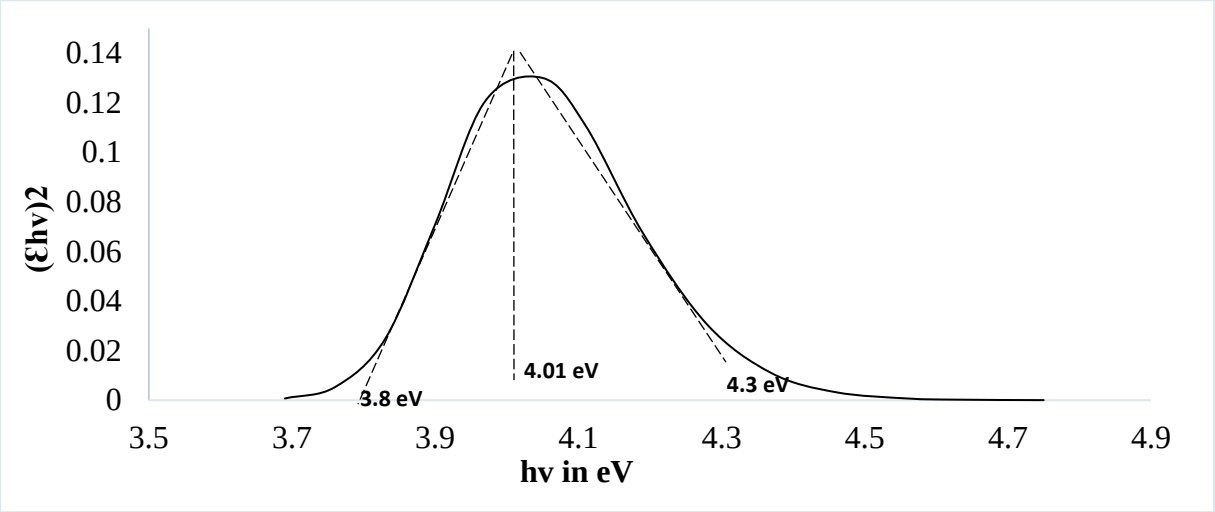

Article DOI: https://doi.org/10.37284/ijar.5.1.677

Data obtained after analysis of $ZnSeO_4$-Hex with Energy Dispersive X-ray Spectroscopy was as presented in *Table 2*.

Table 2: Rayny EDX 800HS data

Sample	Composition %			KeV respectively	
	Zn	Se	O		
QDsS1	40.82	40.43	18.75	8.64	11.2
QDsS2	43.29	42.21	14.50	8.64	11.2

Presented the spectrum in *Figure 5*

EDX data

Figure 5: EDX spectrum for $ZnSeO_4$.Hex (QDsS1 and QDsS2) QDs

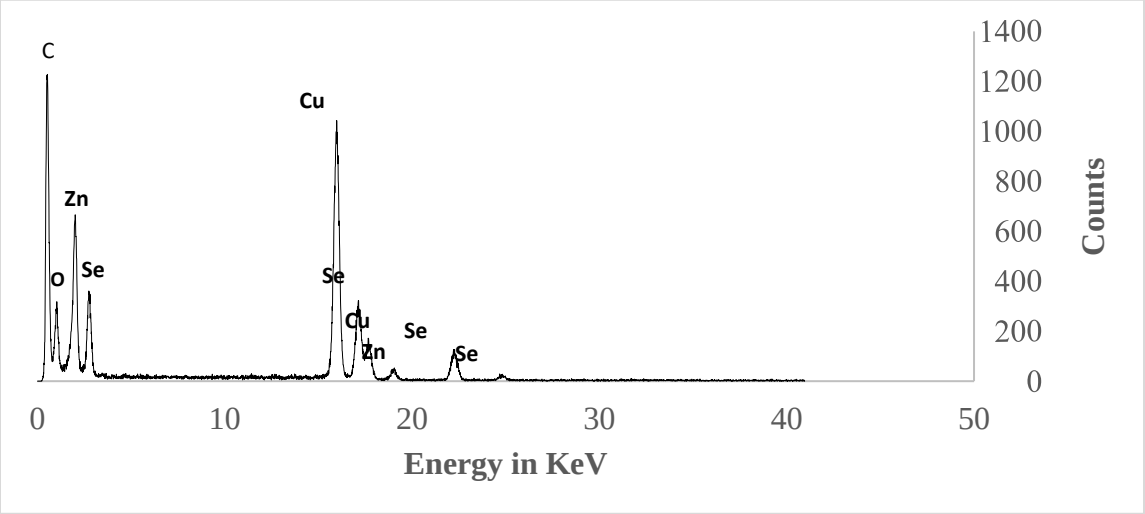

TXRF data

Total X-ray Fluorescence Spectroscopy (TXRF) results for $ZnSeO_4$-Hex (QDsS1 and QDsS2) were as presented in *Table 3* and in the spectra of Figure(s) 5 and 6. The percentages for Zn and Se were prominent as expected.

Table 3: TXFS data

Samples	Composition %			KeV	
	Zn	Se	O		
QDsS1	**41.79**	**40.92**	**17.29**	**8.64**	**11.2**
QDsS2	**42.87**	**41.50**	**14.63**	**8.64**	**11.2**

Spectrum for QDsS1 ($ZnSeO_4$-Hex; crystallite size 8.6 nm) as obtained from S2 PICOFOX TXRF spectrometer was as presented in *Figure 6*.

Article DOI: https://doi.org/10.37284/ijar.5.1.677

Figure 6: The TXFS spectrum for QDsS1 ($ZnSeO_4$-Hex; 8.6 nm crystallite size) QDs

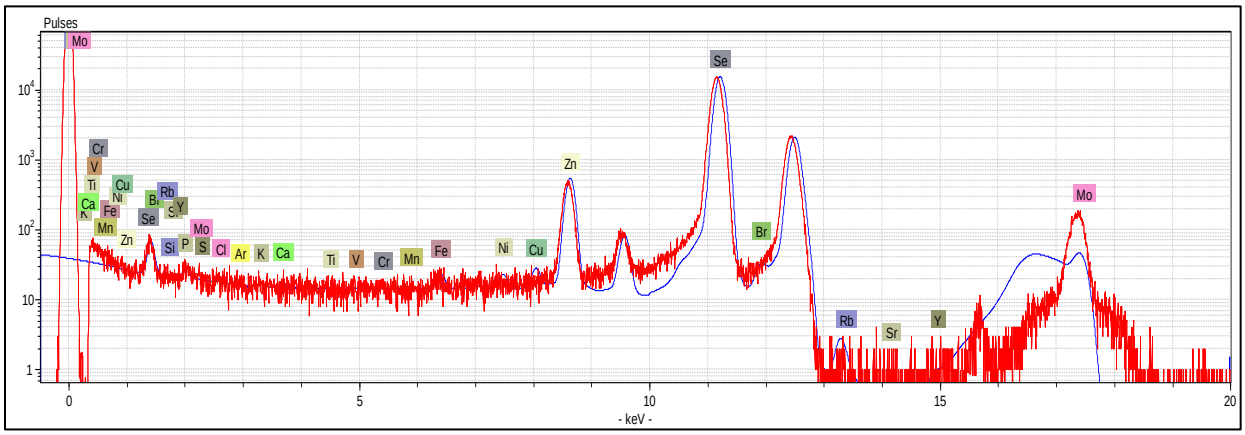

The spectrum for QDsS2 ($ZnSeO_4$-Hex; crystallite size 14.0 nm) obtained on S2 PICOFOX TXRF spectrometer was as presented in *Figure 7*.

Figure 7: The TXRF spectrum for QDsS2 ($ZnSeO_4$-Hex; 14.0 nm crystallite size) QDs

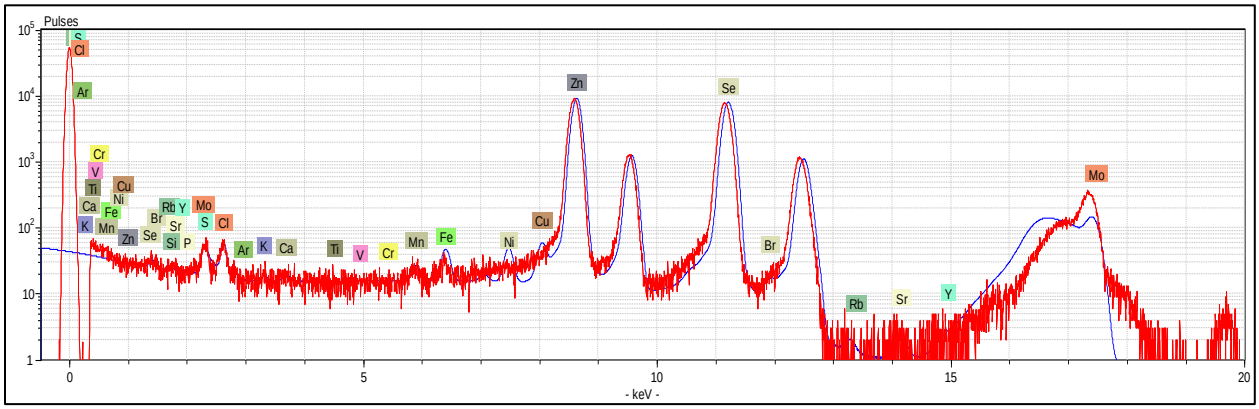

GC-MS data

The data obtained after analysis with Gas Chromatography – Mass Spectroscopy (GC-MS) were shown in *Figure(s) 8* and *9*.

Figure 8: GC-MS spectrum for the $ZnSeO_4$-Hex QDs

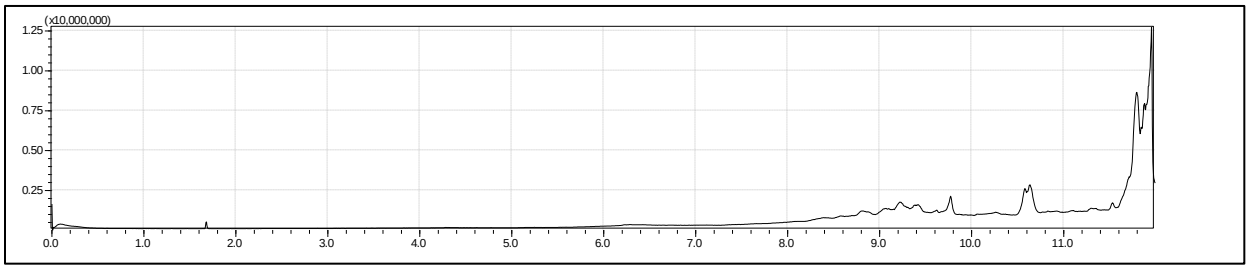

The fragmentation pattern for *Figure 7* was as presented in *Figure 8*.

Article DOI: https://doi.org/10.37284/ijar.5.1.677

Figure 9: GC-MS mass spectrum for $ZnSeO_4$-Hex QDs

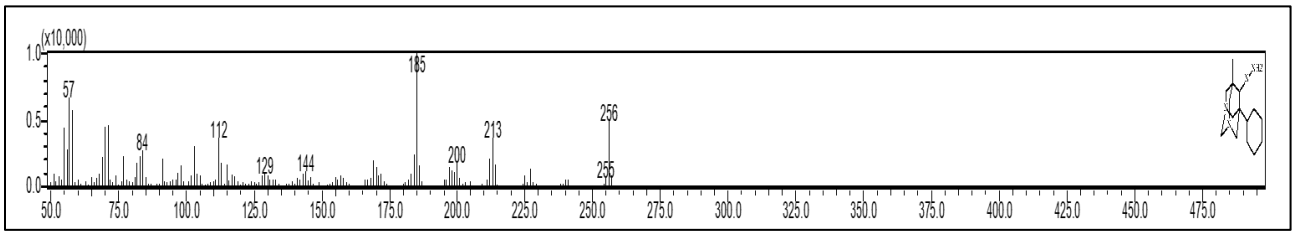

The compound similar to fragmentation pattern in *Figure 8*, above was identified using the library of compounds in the GC-MS. The compound's moiety, containing nitrogen atoms was a closer match to that of hexamine as shown in *Figure 10*.

Figure 10: Compound identified to match the hexamine moiety part in QDs Spectrum; 5-Methyl-7-phenyl-1, 3-diazaadamantan-6-one Hydrazone.

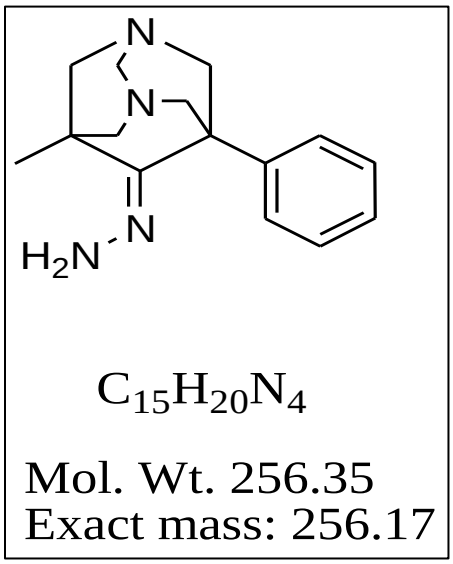

Envisaged structural orientation for $ZnSeO_4$-Hex is as presented in **Figure 11**.

Article DOI: https://doi.org/10.37284/ijar.5.1.677

Figure 11: Envisaged 2D hexagonal structure of the capped QDs using our TEM experimental data

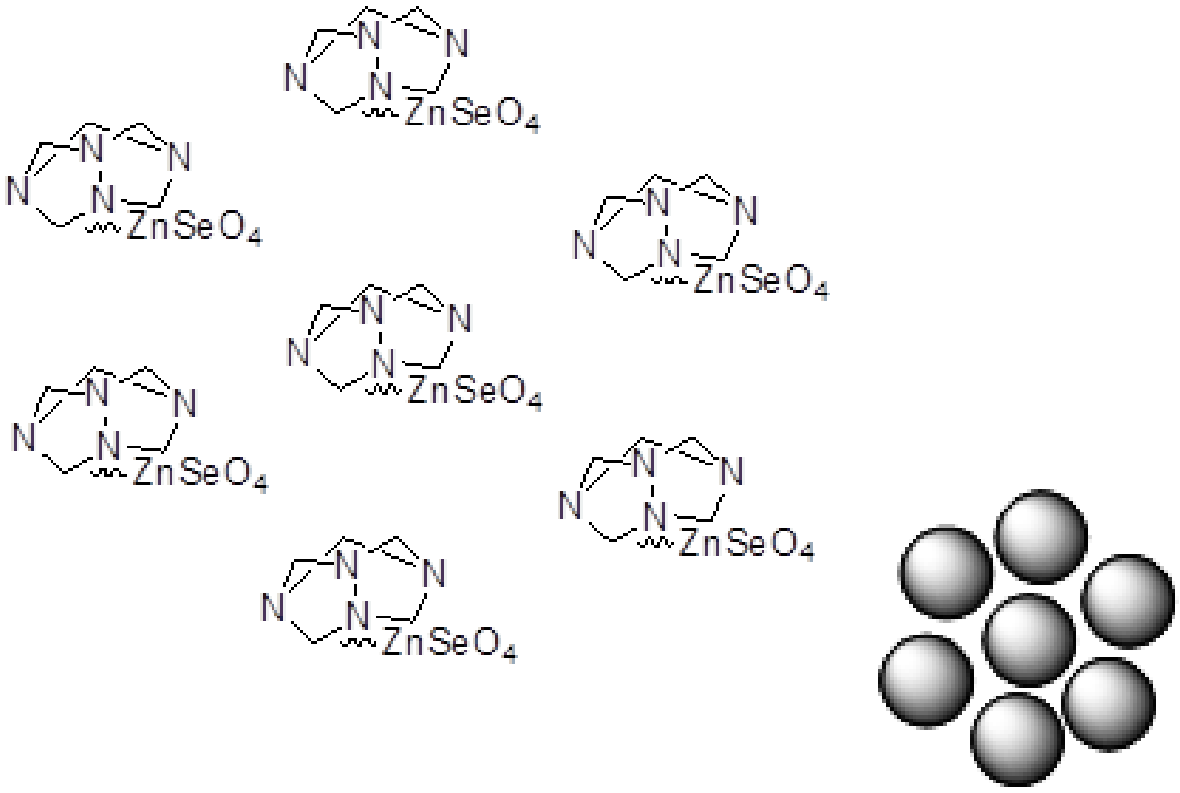

FTIR data

Fourier Transform Infra-red spectrum for $ZnSeO_4$-Hex was as shown in *Figure 12*.

Article DOI: https://doi.org/10.37284/ijar.5.1.677

Figure 12: Fourier transform infra-red spectrum for $ZnSeO_4$-Hex in KBr

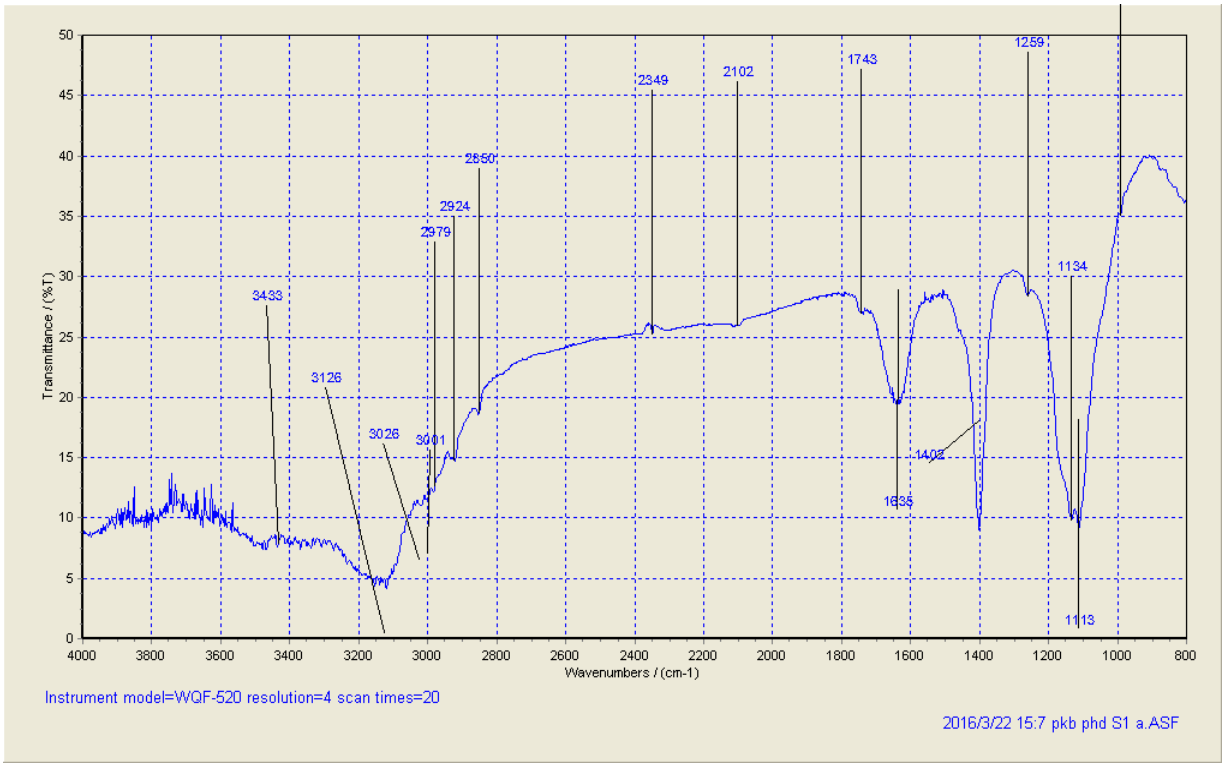

Analysing the FTIR spectrum for QDs, the intense vibrational bands between 2200 and 1200 cm-1 are typical of aromatic ring. This attributes to the ring structure of hexamine. At 3433 and 1635 cm-1 it is the stretching N-H bond and 3126 cm-1 and 1743 cm-1is attributed to C-N stretching. The transmission peak at 2979 cm-1 is for C-H stretching; 2924 non-symmetrical and 2850 cm-1 symmetrical stretching for -CH. The peak at 1259 cm-1 is for –CH2 symmetrical stretching. The intense peak at 1402 cm-1 shows -N-H bending vibration. The 1134 and 1113 cm-1 doublet show C-N and N-H stretching. These vibrational modes observed indicated the presence of hexamine on the surface of $ZnSeO_4$ QDs. The GC-MS and FTIR confirmed the presence of hexamine moiety and Energy Dispersive X-ray (EDX), X-ray Radiation Diffraction (XRD) and Total Fluorescence X-ray (TFXS) spectroscopic analytical techniques and Transmission Electron Microscopy (TEM) confirmed the presence of $ZnSeO_4$ as constituents of the QDs.

TEM data

The Transmission Electron Microscopy analysis images were as presented in *Figure 13*.

Article DOI: https://doi.org/10.37284/ijar.5.1.677

Figure 13: Transmission Electron Microscopic (TEM) images for $ZnSeO_4$-Hex.

(1) **(2)** **(3)**

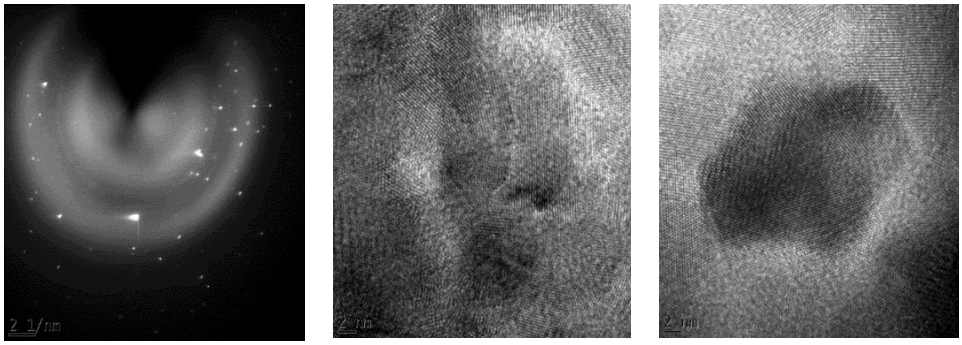

(4)

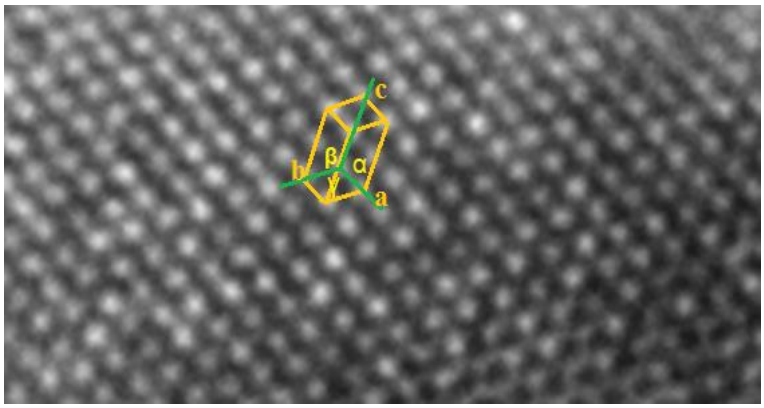

1) is the SAED image, 2) shows 2 nm magnification of crystallites arrangement indicating tilted boundary folds 3) Image showing crystallite boundaries and 4) Enlargement of a section of 3 above, showing hexagonal close packed (hcp) crystal arrangement and inset; Bravais parameter; Primitive unit cell Hexagonal (P) of: $a = b \neq c; \alpha = \beta = 90^{0}; \gamma = 120^{0}$

The Selected Area Electronic Diffraction (SAED) image (1) above shows polycrystalline material with hexagonal arrangement. Images 2 show crystal pattern with boundaries and 3 show crystal patterns with tilted fold at the boundaries – this too indicated polycrystalline nanostructures. Image 4 was a section enlargement of image 3 of Figure 13 – so as to illustrate the hexagonal close packed (hcp) arrangement of the crystals in the nanomaterial and Bravais parameter structure for the QDs.

As the enlargement in *Figure 13(4)* illustrate, the nanoparticles had hexagonal close packing (hcp) of high symmetry. On the unit cell it is illustrated how a = b ≠ c and α= β≠γ, which is typical of hexagonal crystal system.

X-ray data

X-ray Diffraction re-plotted spectrum was as presented in *Figure 14.*

Article DOI: https://doi.org/10.37284/ijar.5.1.677

Figure 14: The x-ray diffraction pattern for $ZnSeO_4$-Hex

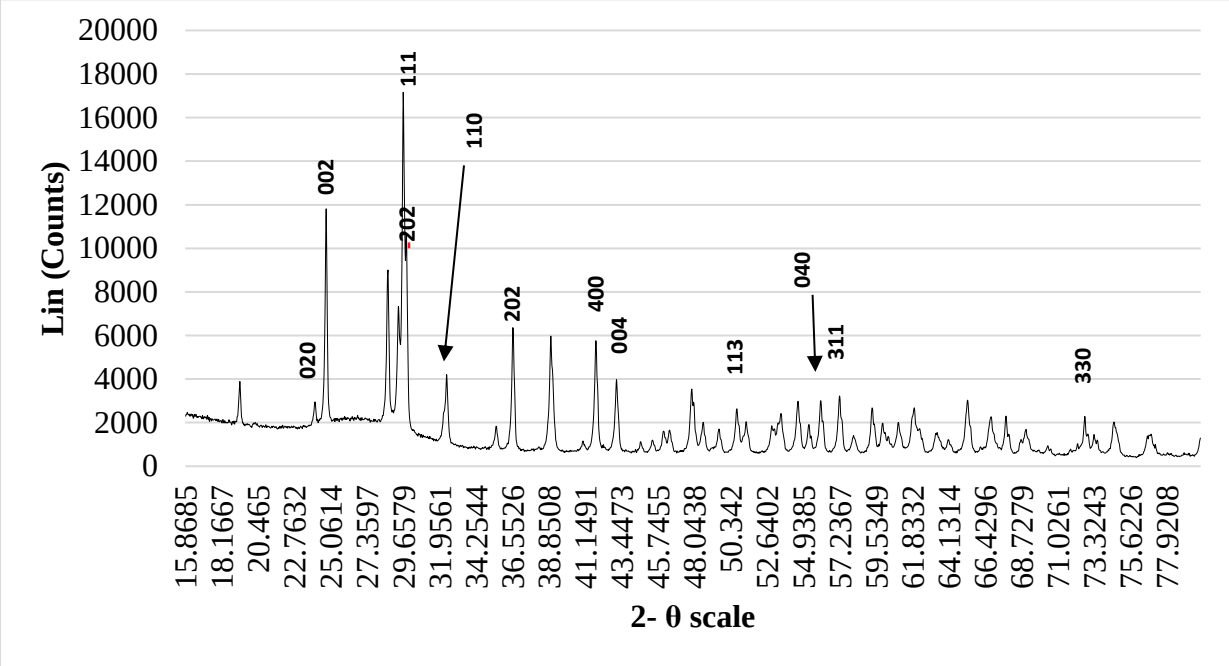

The diffraction pattern typically shows that of microcrystalline nanoparticles. It can be noted that the peaks are relatively broad and the broadening is fairly consistent, and the peaks are also sharp, showing presence of nano-sized material of crystallite size less than 100 nm (Dorofeev et al., 2012). Using XRD pattern at given theta, d_{hkl} (Å) values were calculated using the Scherer equation 3. The letters; *hkl* denote miller indices. Miller indices leads one to describe the arrangement of atoms within a unit cell. When the unit cell is known, the distance between atoms and the force binding them can be calculated. The force holding the lattice determine which type of electrons can participate in conduction process. As mentioned in the abstract, QDsS1 and QDsS2 had the same chemical constituents, which was elucidated in this research as $ZnSeO_4$ –Hex, but different crystallite sizes; – that for QDsS1 had average crystal size of 8.6 nm absorbing at 202 nm and QDsS2 average size of 14.0 nm absorbing at 302 nm. Presented in Table 4 are d_{hkl} (Å) and miller indices for X-ray diffraction patterns for the two crystallites calculated using Equation 3.

$$d_{hkl} = \frac{\lambda}{2 \sin \theta} \quad (3)$$

Where; d_{hkl} = the distance of diffracting crystal lattice plane, *hkl* = miller indices in those planes; θ = the diffraction angle; λ = the x-ray wavelength

The miller indices; *hkl* (a set of numbers which quantify the intercepts and are usually used to identify the crystal plane or surface), these miller indices were assigned to the diffraction patterns by comparison with JCPDS files in literature and they were as presented in Figure 13. Calculated lattice parameters were; a = b = 5.9855 Å and c= 7.1887 Å; c/a = 1.2010 Å and volume per unit cell was 223.03 $Å^3$

Evaluation of Sensing Data

After characterization of the QDs, absorption and fluorescence analyses for their sensing capability were carried out.

Absorbance of QDs with neat pollutants data

The spectra for neat pollutants with QDs were obtained for the purpose of identifying characteristic peaks formed after interaction. These absorption spectra were as presented in *Figure 15*; - on the right side of Figure 15, the spectra labelled 1, representing interaction of the QDs with ANTH, labelled 2 show their interaction with BaP; the

Article DOI: https://doi.org/10.37284/ijar.5.1.677

spectra labelled 3 showing interaction of the nanoparticles with PRN and those labelled 4 show interaction of the QDs with pyridine.

Figure 15: Absorption spectra for interaction of QDsS1 (left hand side) and QDsS2 (on the right-hand side) with neat pollutants

	Sensor QDsS1 with pollutant	Sensor QDsS2 with pollutants
1.	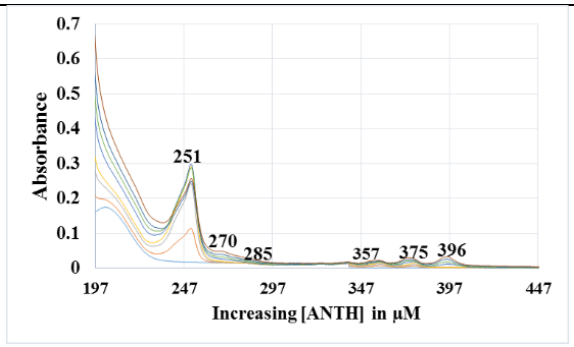	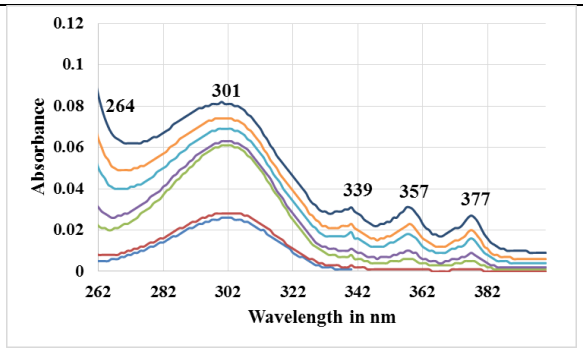
2.	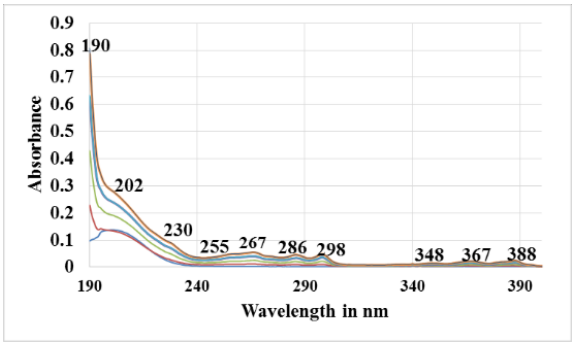	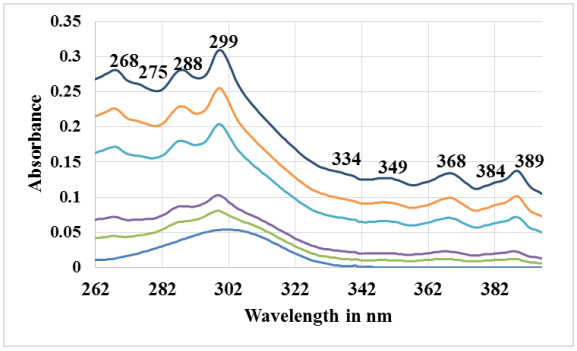
3.	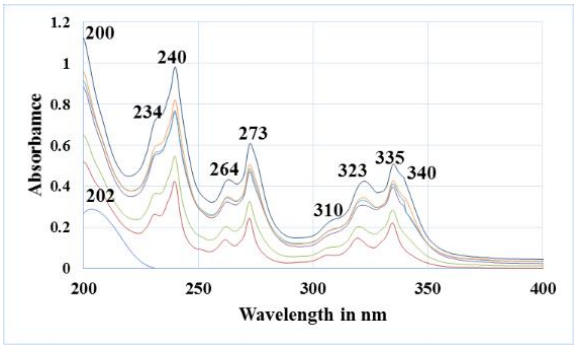	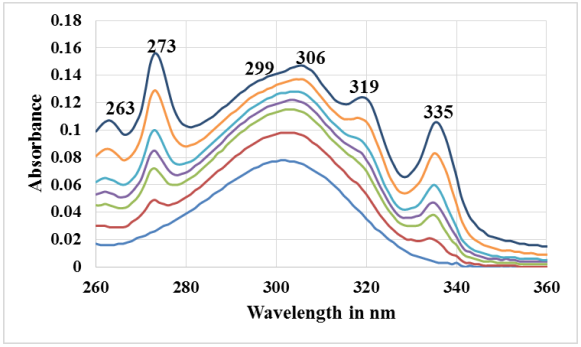

Article DOI: https://doi.org/10.37284/ijar.5.1.677

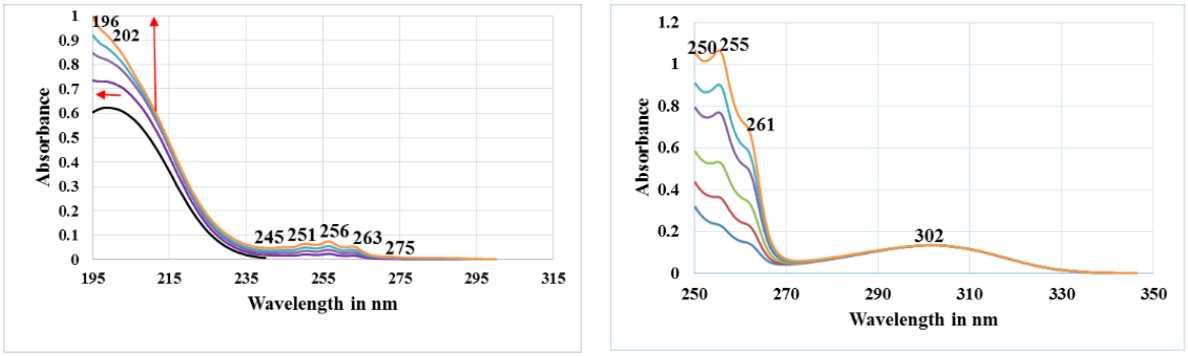

4.

1) ANTH, 2) BaP, 3) PRN and 4) py

The absorption spectra for QDsS1 and QDsS2 with the neat pollutants clearly show the characteristic changes the pollutants have caused within the spectra for the sensing reagents after interaction. Interaction of QDsS1 with BaP forms new peaks at 190, 255, 267, 286, 298, 348, 367 and 388 nm; the peak for the sensor still appears at 202 and keeps increasing in intensity and a new shoulder peak at 230 nm. When QDsS1 interacted with py, there was a shift of the sensor peak from 202 to 196 nm, more towards the blue end of the electromagnetic spectrum and the characteristic peaks for py aside the one at 202 that shifted to 200 nm. The characteristic peaks for BaP can be observed. Interaction of QDsS2 with ANTH shows increasing absorbance for the peak of the sensing particle at 301 nm and the characteristic peaks for ANTH too increasing in intensity, though with some missing peaks – those at 296, 309 and 324 nm. After interaction of QDsS2 with BaP, three new peaks at 275, 334, and 384 aside the characteristic peaks for the sensor and some of BaP were observed. It was observed that, after interaction of QDsS2 with PRN four new peaks in addition to the sensor peak appeared in the spectrum. It was also observed that the sensor reagent's peak shifted towards the red end of the electromagnetic spectrum to 306 nm from 301 nm.

Fluorescence with Pollutants

Fluorescence analysis spectra for neat pollutants with QDsS1 and QDsS2 were obtained following the procedure described in the methodology section and they were as presented in *Figure 16*.

Figure 16: Fluorescence spectra for interaction of QDsS1 (on the left-hand side) & QDsS2 (on the right-hand side) with neat pollutants,

QDsS1 fluorescence with pollutants	QDsS2 fluorescence with pollutants

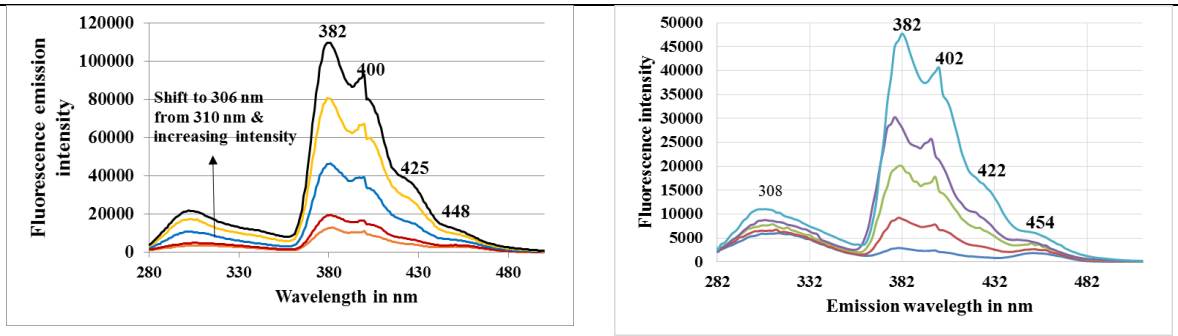

1.

Article DOI: https://doi.org/10.37284/ijar.5.1.677

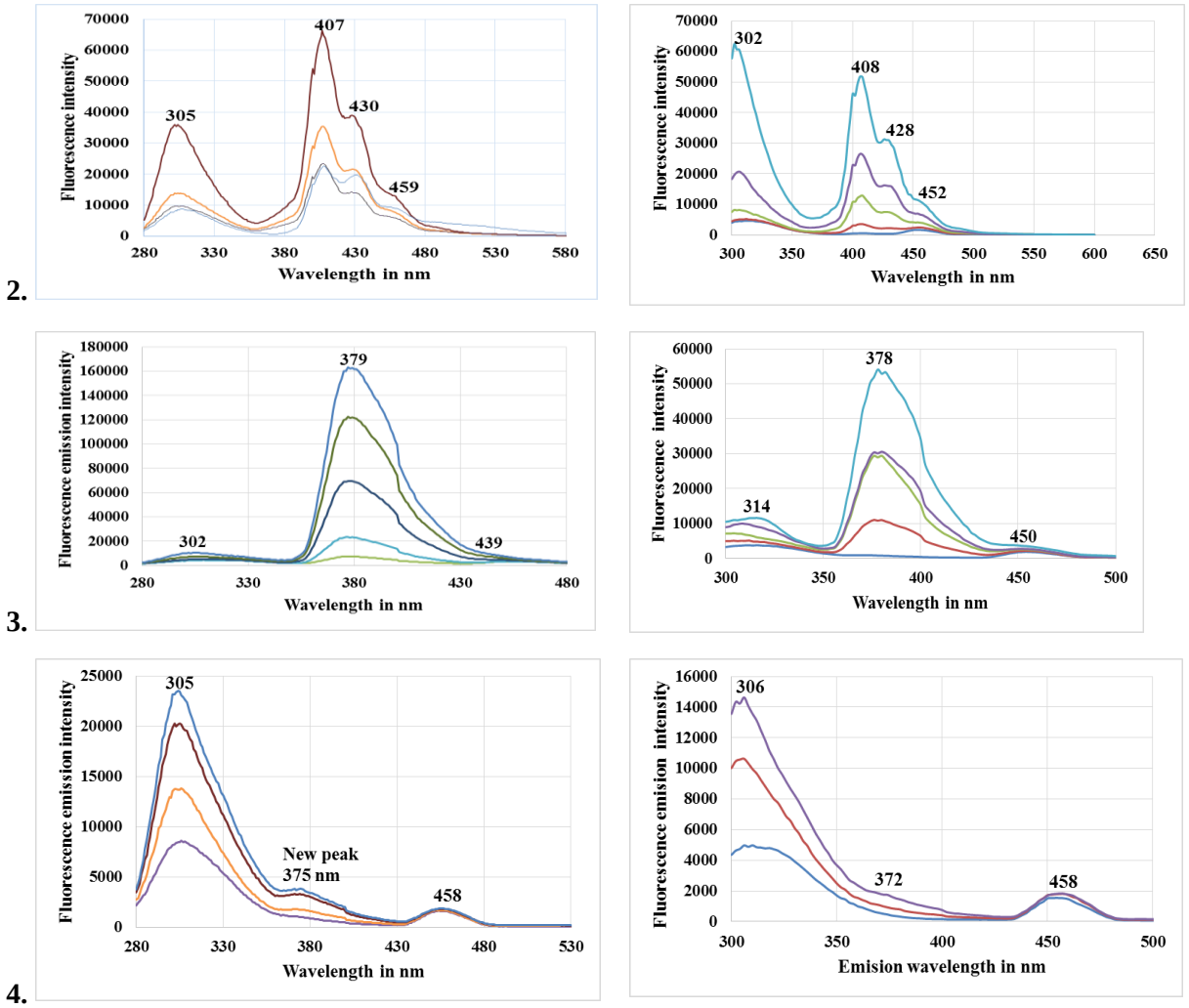

1) ANTH 2) BaP 3) PRN and 4) py (QDsS1 and QDsS2 were elucidated as $ZnSeO_4$-Hex of two crystal sizes).

As presented in *Figure 16*, labelling 1, shows spectra for interaction of QDsS1 (($ZnSeO_4$ – Hex; 8.4 nm size) with ANTH - left side; and to the right QDsS2 ($ZnSeO_4$ – Hex; 14.0 nm size) with ANTH. The labelling 2, is for BaP interaction with QDsS1 (($ZnSeO_4$ – Hex; 8.4 nm size) and QDsS2 ($ZnSeO_4$ – Hex; 14.0 nm size); QDsS1 on the left as titled and QDsS2 ($ZnSeO_4$ – Hex; 14.0 nm size) on the right side as titled above. Finally, 3 and 4 are spectra for interaction of QDsS1 (($ZnSeO_4$ – Hex; 8.4 nm size) and QDsS2 ($ZnSeO_4$ – Hex; 14.0 nm size) with PRN and py respectively – showing QDsS1 (($ZnSeO_4$ – Hex; 8.4 nm size) on the left side and QDsS2 ($ZnSeO_4$ – Hex; 14.0 nm size) on the right side as shown above.

Sensors with neat pollutants' absorption calibration plots

As stated earlier in methodology section, calibration plots were obtained and were used for estimation of pollutants in environmental samples. Presented in Figure 17 are the absorption calibration plots for interaction of sensor nanoparticles with pollutants (ANTH, BaP, PRN and py).

Article DOI: https://doi.org/10.37284/ijar.5.1.677

Figure 17: Absorption calibration plots for interaction of QDsS1 and QDsS2 ($ZnSeO_4$-Hex) with neat pollutants: 1) ANTH 2) BaP 3) PRN and 4) py

	QDsS1 with pollutants	QDsS2 with pollutants
1.	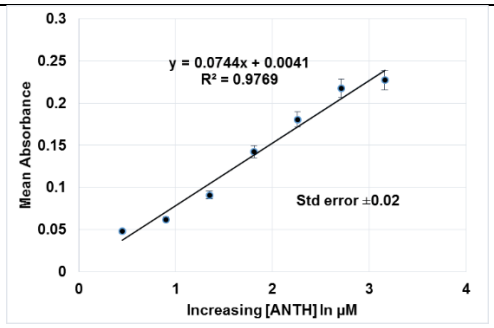	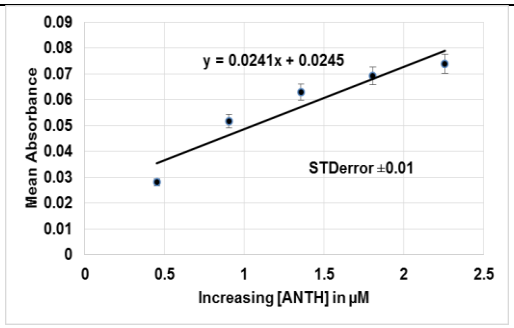
2.	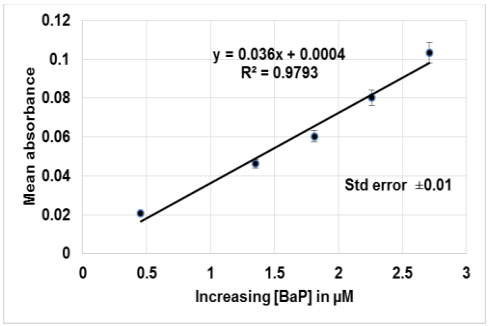	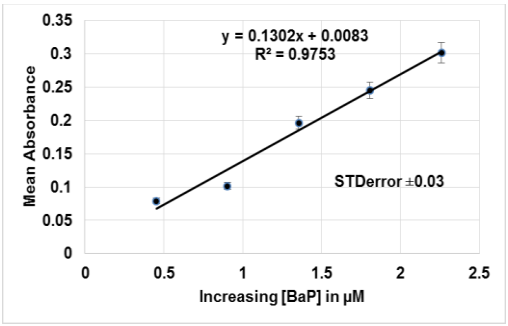
3.	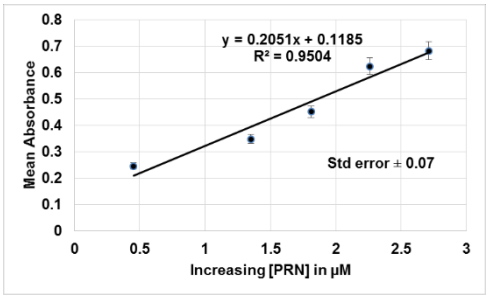	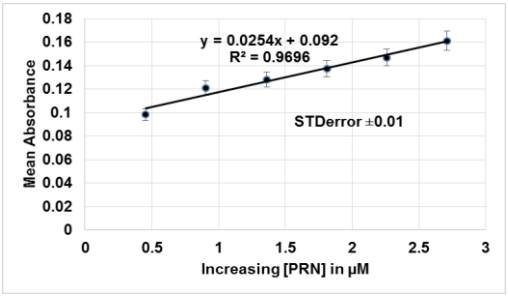
4.	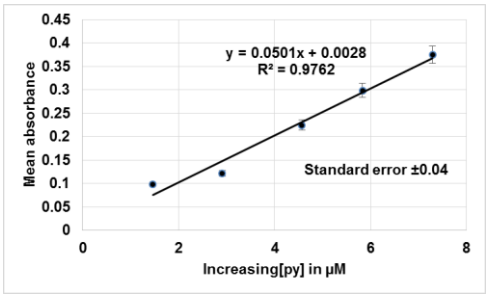	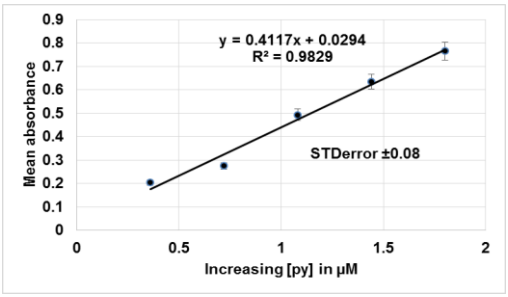

Sensors with neat pollutants' fluorescence calibration plots

The calibration plots for the sensors and neat pollutants are as presented in *Figure 18*.

Article DOI: https://doi.org/10.37284/ijar.5.1.677

Figure 18: Fluorescence calibration plots for interaction of QDsS1 and (QDsS2 ($ZnSeO_4$-Hex) with neat pollutants: 1) ANTH 2) BaP 3) PRN and 4) py

QDsS1 with pollutants	QDsS2 with pollutants
1. 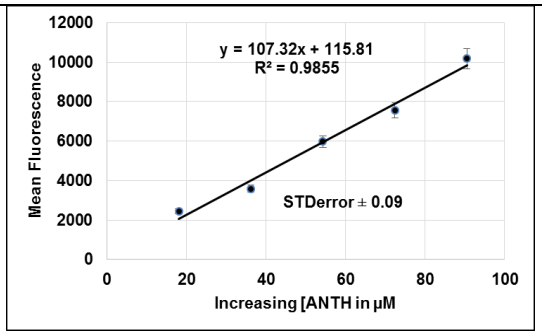	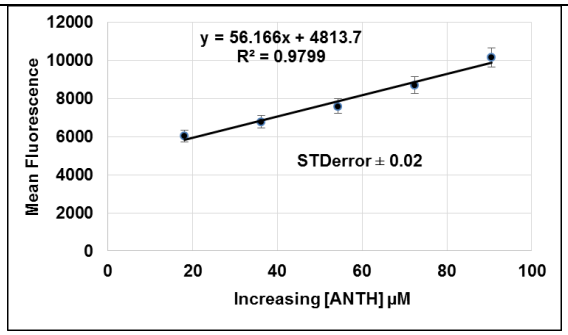
2. 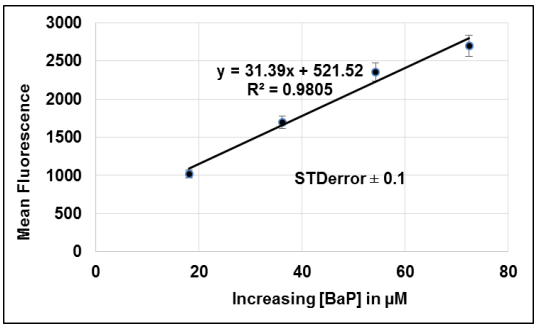	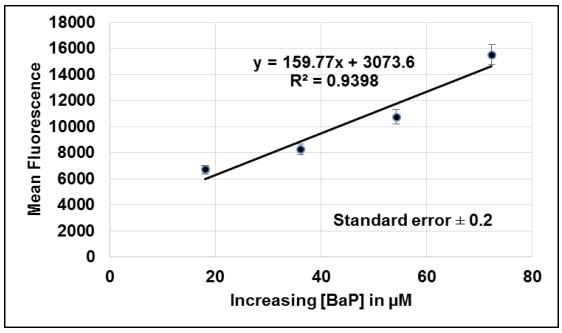
3. 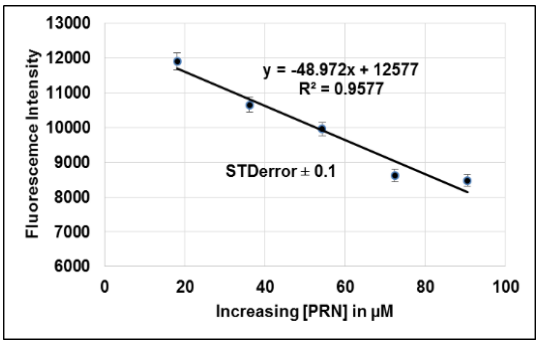	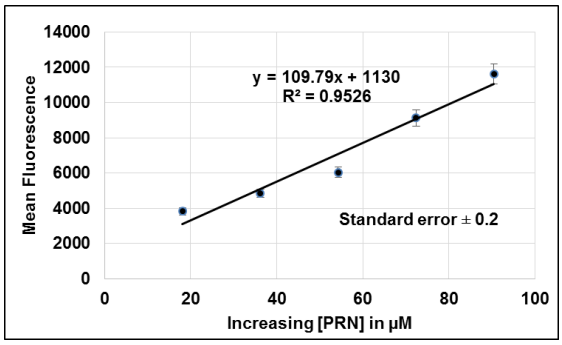
4. 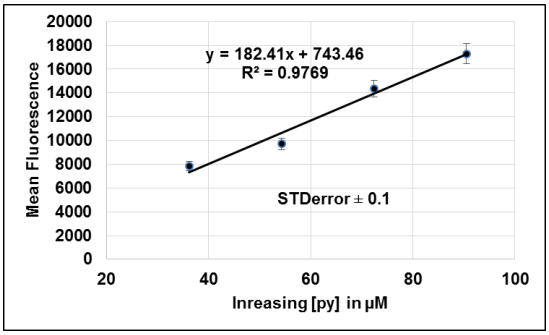	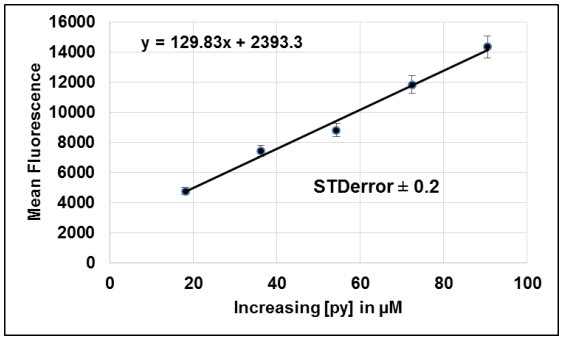

Article DOI: https://doi.org/10.37284/ijar.5.1.677

Absorption data for sensors with cigarette smoke and vehicle exhaust pipe dust extracts

The above calibration plots were used to evaluate the amounts of the carcinogenic compounds in environmental samples, thus in cigarette smoke and diesel engine exhaust pipe dust extracts. The spectra after interaction of the QDs with samples extracted from cigarette smoke and diesel engine vehicle exhaust pipe system as mentioned above were as presented in Figure 19.

Figure 19: Absorption spectra for QDsS1 and QDsS2 ($ZnSeO_4$-Hex) with cigarette smoke and vehicle exhaust pipe extracts (1 and 2).

	QDsS1 with environmental samples	QDsS2 with environmental samples
1.	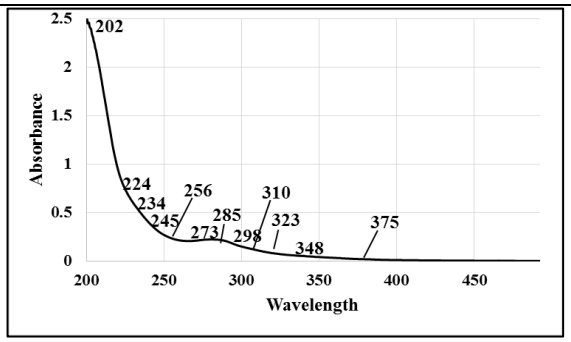	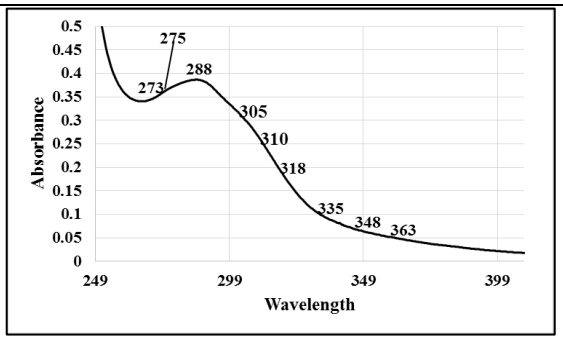
2.	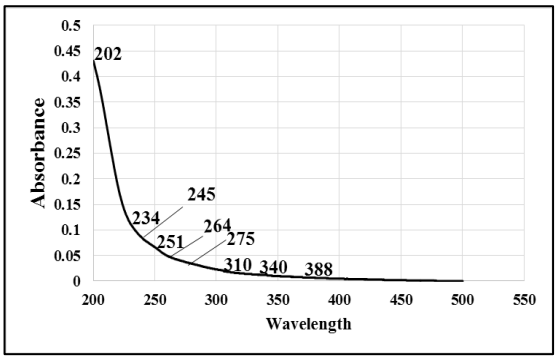	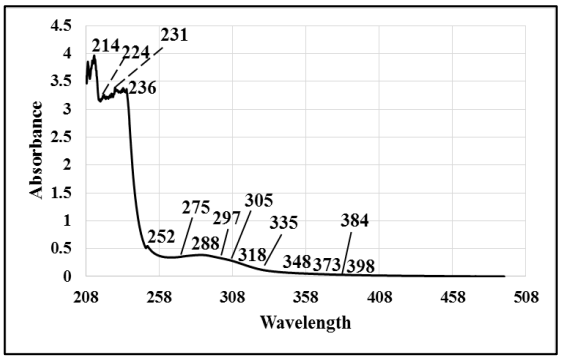

Where '1' is cigarette smoke extract and '2' vehicle exhaust pipe extract.

In *Figure 19(1),* on the left-hand side, is shown the absorption spectrum after interaction of QDsS1 ($ZnSeO_4$-Hex of 8.6 nm size) with cigarette smoke extract - characteristic peaks for ANTH – in the spectrum, were observed at 285 and 375 nm; characteristic peaks for BaP –in Figure 19 appeared at: 202, 256, 285, 298 and 348 nm; those for PRN – identified in spectrum of Figure 19(1), were at 234, 273, 310 and 323 nm and finally for py, peaks at 285 nm and 256 nm were identified. After interaction of QDsS2 ($ZnSeO_4$-Hex of 14.0 nm size) with cigarette smoke extract – in the spectrum, characteristic peaks for BaP were at: 275, 288, 334, 349 and 368 nm; those for PRN were at: 273, 305, 318, 335 and 348 nm; and for py, the peaks observed were: 256 nm and 262 nm.

Quantification of the environmental samples using calibration plots

Quantification of ANTH, BaP, PRN and py in cigarette smoke extract and vehicle exhaust pipe dust extract samples was pecked on the Δ-signal. Thus, the difference between the signals of the main absorption or emission peak of the nano-sensor alone with that of the nano-sensor with pollutants, on which the calibration plots were based. From the calibration plots of the sensor with pollutants, the slope and intercept were used to evaluate the

Article DOI: https://doi.org/10.37284/ijar.5.1.677

unknown concentration of ANTH, BaP, PRN and py in the environmental samples (Equation 4).

$$C_{unknown} = \frac{Signal \quad of \quad C_{unknown} - Intercept}{Slope} \quad (4)$$

In *Tables 4* and *5* are presented the estimated concentration of the environmental samples for absorbance and fluorescence respectively.

Table 4: Absorbance data for QDsS1 and QDsS2 for estimation of (ANTH)1 (BaP)2, (PRN)3& (py)4 in A). Cigarette smoke environmental sample and B). Vehicle exhaust pipe samples, from CBD – NAIROBI:

A			B		
Sensor	Envr. sample signal intercept	Conc./ µg/cig	Sensor	Envr. sample signal intercept	Conc./µg/ mg dust
QDsS1 ($ZnSeO_4$-Hex of 8.6 nm size)	**0.3819[1]**	**9.15[1]**	QDsS1 ($ZnSeO_4$-Hex of 8.6 nm size)	**0.0619[1]**	**0.30[1]**
	0.2086[2]	**14.62[2]**		**0.0446[2]**	**0.63[2]**
	0.3945[3]	**3.89[3]**		**0.0245[3]**	**0.05[3]**
	0.2602[4]	**13.25[4]**		**0.0962[4]**	**0.30[4]**
QDsS2 ($ZnSeO_4$-Hex of 14.0 nm size)	**0.1305[1]**	**9.65[1]**	QDsS2 ($ZnSeO_4$-Hex of 14.0 nm size)	**0.0245[1]**	**0.36[1]**
	0.5617[2]	**10.88[2]**		**0.1887[2]**	**0.73[2]**
	0.0668[3]	**5.32[3]**		**0.0025[3]**	**0.04[3]**
	0.4861[4]	**9.34[4]**		**0.1511[4]**	**0.58[4]**

Table 5: Fluorescence data for QDsS1 and QDsS2 for estimation of (ANTH)1 (BaP)2, (PRN)3& (py)4 in A). Cigarette smoke environmental sample and B). Vehicle exhaust pipe samples, from CBD – NAIROBI:

A			**B**		
Sensor	**Envir. sample signal intercept**	**Conc./µg/cig**	**Sensor**	**Envr. sample signal – intercept**	**Conc./µg/mg dust**
QDsS1 ($ZnSeO_4$-Hex of 8.6 nm size)	41825.2[1]	694.6[1]	QDsS1 ($ZnSeO_4$-Hex of 8.6 nm size)	13096.2[1]	43.5[1]
	3800.5[2]	305.5[2]		23834.5[2]	383.2[2]
	2624.0[3]	108.4[3]		60478.0[3]	499.5[3]
	12669.5[4]	54.9[4]		121913.5[4]	105.7[4]
QDsS2 ($ZnSeO_4$-Hex of 14.0 nm size)	21054.3[1]	668. 1[1]	QDsS2 ($ZnSeO_4$-Hex of 14.0 nm size)	12971.7[1]	21.2[1]
	13656.4[2]	215.7[2]		14091.6[2]	44.5[2]
	17273.0[3]	318.2[3]		10122.0[3]	37.3[3]
	12969.4[4]	71.1[4]		2149.3[4]	2.6[4]

In literature, Satnam et al., (2009), reported ANTH 0.9 µg/cig; BaP 1.4 µg/cig and PRN 2.8 µg/cig.

CONCLUSION

Quantum Dots QDsS1 and QDsS2 which are Zinc Selenate capped with hexamine ($ZnSeO_4$.Hex) with different crystallite sizes; where QDsS1 ($ZnSeO_4$-Hex; size 8.6 nm) and QDsS2 ($ZnSeO_4$-Hex; size 14.0 nm) were successfully synthesized and characterized as presented in this paper. It was established from the experiments carried out in this study that, the sensing reagents QDsS1 ($ZnSeO_4$-Hex of diameter size 8.6 nm) and QDsS2 ($ZnSeO_4$-Hex of diameter size 14.0 nm) showed some specificity, showing characteristic spectra after interaction with individual pollutants identified for this study. QDsS1 ($ZnSeO_4$-Hex of 8.6 nm diameter size) specifically interacted with ANTH, BaP, PRN, and py in cigarette smoke extract and QDsS2

Article DOI: https://doi.org/10.37284/ijar.5.1.677

($ZnSeO_4$-Hex of 14.0 nm diameter size) too specifically interacted with ANTH, BaP, PRN and py in cigarette smoke extract from a matrix containing other PAHs. From the vehicle exhaust pipe dust in ethanol, QDsS1 ($ZnSeO_4$-Hex of 8.6 nm diameter size) and QDsS2 ($ZnSeO_4$-Hex of 14.0 nm diameter size) specifically interacted with ANTH, BaP, PRN and py.

The detection limits (LOD) and quantification limits (LOQ) were relatively low, and some quite low (0.014 – 0.11 µg/L), notably below the permissible exposure limits (PEL) set by international pollution monitoring agencies. These nano-sensors can therefore facilitate detection of micro-concentration of ANTH, BaP, PRN and py. When the calibration plots were used to evaluate the Polycyclic Aromatic Hydrocarbons (PAHs) and py in cigarette smoke and vehicle exhaust pipe dust, it was noted as presented in Table(s) 4 and 5 that, the amounts of these pollutants in the afore mentioned materials, were greater than the amounts for permissible exposure limits as recommended by EPA and WHO. The pollution level for these carcinogenic chemicals released in the environment through cigarette smoking and vehicle emissions is hazardous to health for both active and passive smokers, and those exposed to vehicle exhaust dust. This calls for measures to eliminate or reduce such levels to recommended PEL.

ACKNOWLEDGEMENT

Prof. Bulimo's research crew at KEMRI for their co-operation and support, that enabled us perform fluorescence study. Greatly so, to National Council for Science, Technology, and Innovation (NACOSTI) – Kenya, for financial support – this enabled us reach our goals. Lastly to Jomo Kenyatta University of Agriculture and Technology for facilitating this research and Technical University of Kenya for allowing us use their UV-VIS Spectrophotometer and FTIR Spectrophotometer.

REFERENCES

Analytical detection limit guidance and laboratory guide for determining Method Detection Limits (MDLs) manual – Department of natural resources, Wisconsin USA (April 1996).

Cañizares P and Luque de Castro M.D. Flow-through sensor based on derivative synchronous fluorescence spectrometry for the simultaneous determination of pyrene, benzo(e)pyrene and benzo(ghi)pyrene in water. Fresenius. J. Anal. Chem. 354 (1996) 291 – 295.

Clayton P.M, Vas A.C, T. Bui, Drake F.A and McAdam K. Spectroscopic studies on nicotine and nor nicotine in the UV-region. Journal of organic chemistry: chirality vol. 25 Issue 5 (2013) 265 -311.

Dorofeev G.A, Streletskii A.N, Povstrugar A.V, Protasov A.V and Elsukov E.P. Determination of nanoparticle sizes by the X-ray diffraction method. Colloidal Journal 74(6) (2012).

Elosua C, Bariain C, MatiasI R., Rodriguez A, Colacio E, Salinas-Castillo A, Segura-Carretero A and Fernandez-Gutiérrez A. Pyridine Vapors Detection by an Optical Fibre Sensor. *Sensors 8*(2) (2008) 847-859.

Fernandez-Sanchez J. F.; Carretero A. S.; Cruces-Blanco C. and Fernandez-Gutierrez A. Highly sensitive and selective fluorescence optosensor to detect and quantify benzo(a)pyrene in water samples. Anal. Chim. Acta (2004) 1-7.

Goh G.E and McCormick. Effect of particle size on the UV absorbance of Zinc Oxide nanoparticles. Elsevier; Scripta Materiala Vol. 78 – 79(2014)49 – 52.

G. M. Lohar, S. K. Shinde and V. J. Fulari. Structural, morphological, optical and photoluminescent properties of spray-deposited ZnSe thin film. Journal of Semi-conductors Vol. 35, No. 1 (2014) 11300-1 – 11300-5.

Luca S, Jaqueline P.V, Massimiliano A,Vito L, Gelson P, Eder J.L and Claudio S. Efficient preparation of Zinc Selenates for the synthesis of selenol esters 'on water' conditions. Molecules 22 (2017), 953

Malgorzata S, Malgorzata P, Dobrzynka E, Pyrzynska K and Baraniecka J. Polycyclic Aromatic Hydrocarbons Distribution in Fine and Ultrafine Particles Emitted from Diesel Engines.

Article DOI: https://doi.org/10.37284/ijar.5.1.677

Pol. J. Environ. Stud. Vol. 22, No. 2 (2013), 553-560.

Mosquera E, Carvajal N, Morel M and Marin C. Fabrication of ZnSe nanoparticles: Structural, optical and Raman studies. Journal of Luminescence 192 (2017) 8.14 – 817.

NIOSH Manual for Analytical Methods (NMAM) July issue (1986).

OSHA: Occupational Safety and Health Administration Manual (1996).

Rengarajan T, Rajendran P, Nandakumar N, Lokeshkumar B, Rajendran P, Nishigaki I.Exposure to polycyclic aromatic hydrocarbons with special focus on cancer. Asian pacific journal of tropical biomedicine volume 5, Issue 3 (2015) 182 - 189.

Ripp. J. Analytical Detection Limit Gidance & Laboratory Guide for determining Method Detection Limit (MDL). Wisconsin Department of Natural Resources certification Program (1996) PUBL – TS – 056 – 96.

Powder Diffraction File (PDF) – inorganic compounds JCPDS international center for diffraction data, Philadelphia (1984)

Polycyclic Aromatic Hydrocarbons in cigarette smoke. Satnam S, Vishal A.V and Amjad A. journal of Punjab Academic of Sciences 5-6 (1 & 2) 2008 - 2009

Schmeltz I, Stedman R.L, Chamberlain W.J and Burdick D. Composition studies on tobacco bases of cigarette smoke. Journal of the Science of food and agriculture Vol. 15, Issue 11 (1964) 774 – 781.

Sluszny C; Gridin V. V.; Bulatov V and Schechter I. Polymer film sensor for sampling and remote analysis of polycyclic aromatic hydrocarbons in clear and turbid aqueous environments. Analytica ChimicaActa 522 (2004) 145–152.

Traviesa-Alvarez J.M., Sánchez-BarragánI, Costa-Fernández J. M, Pereiro R and Sanz-Medel A. Room temperature phosphorescence optosensing of benzo(a)pyrene in water using halogenated molecularly imprinted polymers. Analyst, 132, (2007) 218-223.

Wang L, Huang Z, Gao, Q Liu Y, Kou X and Xiao D. A Novel Pyrene Fluorescent Sensor Based on the π - π Interaction between Pyrene and Graphene of Graphene–Cadmium Telluride Quantum Dot Nano composites. Spectroscopy Letters, Volume 48, Issue 10 (2015) 748-756.

